Investigation on the Growth and Characterization of Nonlinear Optical Single Crystals of Tris-Allyl Thiourea Mercury Bromide (ATMB)

I. Vetha Potheher[a], K. Rajarajan[b], M. Vimalan[c], T. Rajesh Kumar[d], R. Jeyasekaran[d] and P. Sagayaraj[d]∗

[a]*Department of Physics, Anna University, Thiruchirapalli, Tamil Nadu, India*
[b]*Department of Physics, R. V. Government Arts College, Chengalpet, Tamil Nadu, India*
[c]*Physics Research Centre, S.T. Hindu College, Nagercoil, Tamil Nadu, India*
[∗d]*Department of Physics, Loyola College, Chennai, Tamil Nadu, India*

_____

Abstract

Single crystal of Tris-allylthiourea mercury bromide (ATMB), a NLO active complex of allylthiourea was grown by slow evaporation technique at 305 K. The structure of the grown crystal was confirmed by single crystal XRD. The composition of the sample was identified by CHN elemental analysis. The optical properties were investigated by FTIR and optical absorption spectroscopic techniques. From the optical absorption spectrum, the cut-off wavelength and energy gap of the sample were found to be 350 nm and 3.9280 eV respectively. The SHG efficiency of ATMB was found to be nearly 3.5 times higher than that of urea. Thermal analysis confirms that the crystal is thermally stable up to 125.11 ˚C. Scanning Electron Microscope (SEM), photoluminescence (PL), dielectric and dc conductivity studies were carried out and reported for the first time.

Key words : Allylthiourea, Organometallic, Slow evaporation, Photoluminescence, Scanning electron microscope.
_____

INTRODUCTION

With the introduction of the double-radical model, scientists working in the field of NLO materials have developed a series of novel metal organic compounds. This model encourages the inclusion of organic conjugated molecular groups in the distorted polyhedron of co-ordination complex [1]. These complexes have considerable high NLO coefficient (contrast to inorganic material), stable physicochemical properties and better mechanical intention (contrast to organic materials). Under the guidance of this theory, our research group as well as Chinese research
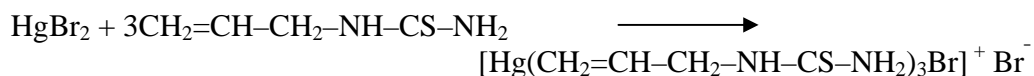
_____

groups have successfully developed and reported few interesting complexes of allylthiourea along with the complexes of thiourea and thiocyanate [2-5]. The structure radical of the organometallic complex, especially in allylthiourea is no longer planar as the benzyl ring, hence the anisotropy of the crystal is reduced as compared with the organic crystals [5]. A comparatively high optical nonlinearity in these complexes comes from the distortion of the tetrahedron, which is composed of three allylthiourea ($C_4H_8N_2S$, AT) and one Cl (or Br) combining with Cd (or Hg). In this context, with AT acting as a ligand, scientists have developed tri-allylthiourea cadmium chloride (ATCC), tri-allyl thiourea zinc chloride (ATZC), tri-allylthiourea cadmium bromide (ATCB), tri-allylthiourea mercury chloride (ATMC) and tri-allylthiourea mercury bromide (ATMB) [6-9]. Tri-allylthiourea mercury bromide (ATMB) is an interesting organometallic complex material designed and synthesized by Hou Wenbo et al [5]. A relatively large susceptibility in ATMB comes from the distorted tetrahedron arrangement in its structure. The complex cation $[HgBr(AT)_3]^+$ forms a distorted tetrahedron using metal ion Hg^{2+} as a centre ion to connect with Br^- and three sulphur atoms in the allylthiourea molecules. The distorted tetrahedron arrangement increases the asymmetric structure and thereby contributes to the enhanced NLO activity. The same has been confirmed in the other complexes of allylthiourea and they possess higher SHG efficiency than both KDP and urea [7, 12]. Deviated from the earlier work, the present article deals with the growth of ATMB by slow evaporation technique instead of the slow cooling technique. The grown crystal was confirmed by single crystal XRD, FTIR and CHN analysis. The grown crystals were also characterized by optical absorption and TG-DTA techniques. Scanning Electron Microscope (SEM), photoluminescence (PL), dielectric and *dc* conductivity studies of ATMB were under taken and reported for the first time. The NLO properties of the grown sample were investigated by Kurtz and Perry powder technique and damage threshold measurement.

MATERIALS AND METHODS

2. Experimental Procedure
2.1 Crystal Growth
ATMB was synthesized by reacting allylthiourea with mercury bromide (AR grade with purity $\geq$ 98 %) in double distilled water. The chemical reaction is as follows:

$$HgBr_2 + 3CH_2=CH-CH_2-NH-CS-NH_2 \longrightarrow [Hg(CH_2=CH-CH_2-NH-CS-NH_2)_3Br]^+ Br^-$$

The solution was stirred continuously for few hours in a beaker and the content was closed with a perforated lid to initiate nucleation at room temperature. During this period, few drops of HBr were slowly added into the solution in order to adjust the pH between 2 and 3. We have observed the formation of only the precipitate, if the pH lies below or above the recommended value [6]. Seed crystals are observed within a week time and they appear as transparent tiny crystals with square shape. The seed crystal was suspended into the solution to initiate further growth. Though the crystal was highly transparent during the initial stages, its transparency was gradually lost after its complete growth. The crystal appeared with light milky white patches and single crystal of dimension 10 x 10 x 7 mm^3 was obtained by slow solvent evaporation technique in a period of 35 – 40 days. Fig. 1 shows the photograph of as grown single crystals of ATMB. It is evident from the photograph that the crystals are developed with sharp edges and layered growth is

172

_____

clearly visible in the SEM micrograph. Thus, the present work indicates that the crystal shape is better controlled under slow evaporation technique than the slow cooling technique used in the past [5].
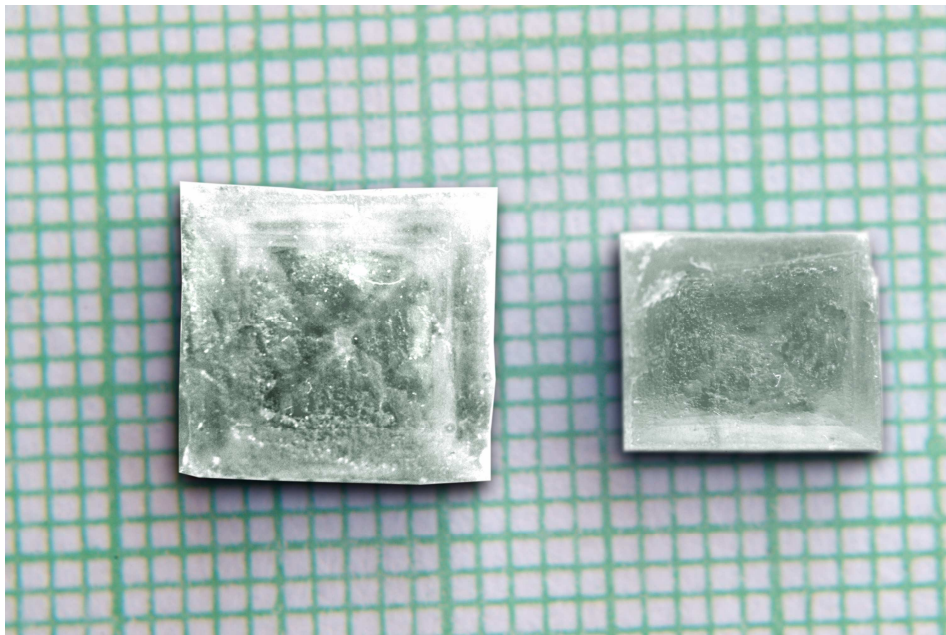

Fig. 1. The photograph of as grown single crystals of ATMB

2.2 Characterization

Single crystal X-Ray diffraction analysis was done with ENRAF NONIUS CAD4-F diffractometer employing MoK$_\alpha$ source. The structure was solved by the direct method and refined by full matrix least square technique using the SHELXL program. Fourier Transform Infrared spectrum (FTIR) of the sample was recorded in the range 4000 – 400 cm^{-1} using AVATAR 330 FT-IR spectrometer. The absorption spectrum of the sample was recorded from 200 nm to 2500 nm using HITACHI U-2800 spectrophotometer. The band gap energy of the sample was calculated using the relation, E = hν eV, where h is Planck's constant and ν = c / λ. The thermal behaviour of the grown crystals was investigated by Perkin Elmer Thermal Analyzer in nitrogen atmosphere at a heating rate of 15 ^{o}C/min from 28 to 1000 ^{o}C. The elemental analysis of ATMB was performed using Elementar Vario EL III Elemental analyzer. The SHG efficiency of ATMB was measured using Kurtz and Perry powder technique [10]. The surface morphology of the as grown sample of ATMB was investigated using a JEOL/EO-JSM-5610 Scanning Electron Microscope (SEM). Photoluminescence of the sample was recorded by VARIAN spectrometer with 2.5 kV fluorescence lamp. Microhardness was measured using a Leitz Wetzlar Vickers microhardness tester fitted with a Vickers diamond pyramidal indenter attached to an incident light microscope. Dielectric constant and dielectric loss of the sample were measured at different temperatures using HIOKI 3532-50 LCR HITESTER in the frequency range from 50 Hz – 5 MHz. The measurement of *dc* electrical conductivity was done using the conventional two-probe technique for temperatures ranging from 313 to 423 K.

_____

RESULTS AND DISCUSSION

3.1 X-Ray Diffraction Analysis

The X-ray diffraction studies confirm the trigonal crystal system of ATMB with non-centrosymmetric space group R3c. The cell parameters, a = b = 11.392 Å, c = 28.692 Å and V = 3323.5806 $Å^3$ are in fairly agreeing with the reported data [5].

3.2 FTIR Analysis

The FTIR spectrum of ATMB single crystal is presented in Fig. 2. It is well known that the AT derivatives are highly favoured in sulphur coordination to the metal during complex formation. From the spectrum, it is evident that the CN stretching frequency gets shifted towards high frequency region by 9 cm^{-1} whereas, the stretching frequency of CS is drastically lowered by 66 cm^{-1} when compared to AT. These observations strongly indicate the probability of coordination of sulphur with mercury in the resulting compound.
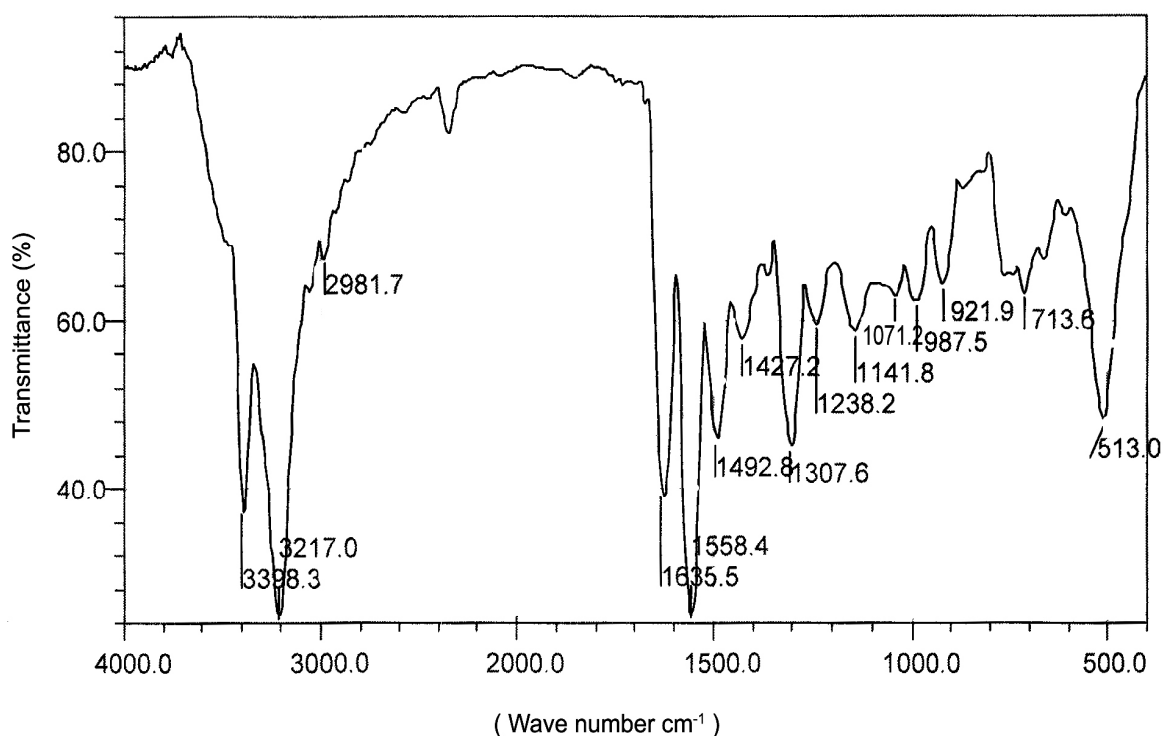

Fig. 2. FTIR spectrum of ATMB single crystal

3.3 Elemental Analysis

The percentage of carbon, hydrogen and nitrogen was determined using the elemental analysis. The presence of the carbon, hydrogen and nitrogen was estimated as 19.86, 3.28 and 11.05 % respectively and they are fairly matching with the theoretical values (20.34, 3.39 and 11.86 %).

_____

3.4 Optical Absorption Studies

Fig. 3 shows the UV-Vis-NIR spectrum along with the Tauc's plot [11] of ATMB single crystal. The UV cut-off wavelength of the sample is seen around 350 nm and the absorption of ATMB is very low in the region from 350 – 2500 nm. The absence of absorption in the above region reveals the suitability of the sample for NLO applications. Using the Tauc's relation, a graph has been plotted between $h\nu$ and $(\alpha h\nu)^2$ to estimate the direct band gap value, where α. is absorption coefficient and $h\nu$ is the energy of the incident photon $(E = h\nu)$. The energy gap (E_{gd}) is determined by extrapolating the straight line portion of the curve to $(\alpha h\nu)^2 = 0$. From the plot, the band gap of ATMB is found to be 3.9280 eV.
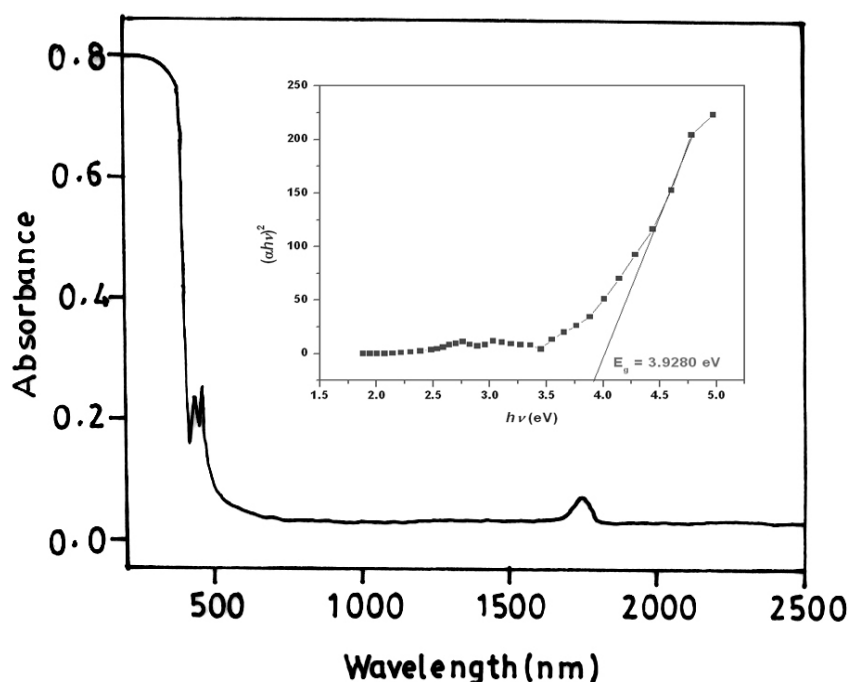

Fig. 3. Absorption spectrum along with the Tauc's plot of ATMB single crystal

3.5 NLO Property

Nonlinear optical property of the sample was studied by Kurtz and Perry powder technique and the efficiency of the sample was compared with microcrystalline powder of KDP and urea. A Q-switched, mode locked Nd:YAG laser operating at the fundamental wavelength of 1.064 µm was used. In the present investigation, the laser pulse of 8 ns with spot radius of 1 mm was employed. The input laser beam was passed through the IR reflector and then directed on the microcrystalline powdered sample packed in a capillary tube. When a laser beam of 1.35 mJ was passed through the sample, second harmonic signal of 532 nm was generated and the output voltage of 55 mV, 520 mV and 1830 mV were obtained from KDP, urea and ATMB respectively. The experimental data show that the second harmonic efficiency of the sample is nearly 3.5 times than that of urea, which is better than ATCC [12] and ATZC [7]. The laser damage threshold measurement of ATMB was carried out using single shot mode setup and it

_____

was found to be about 10.68 GW / cm^2. The value of damage threshold is better than other NLO materials such as MMTC, KDP, urea and BBO [13-15].

3.6 Thermal Analysis

The TG-DTA thermogram of ATMB was recorded and displayed in Fig. 4. The TGA trace confirms that there is no water of crystallization before the decomposition of the sample. During the first stage of decomposition, there is a weight loss of about 12 %, which is probably be due to the loss of Br atom. In the successive stage, the three molecules of allylthiourea (AT) are lost whose weight percentage (48%) is comparable with the theoretical value of three molecules (49.165%) of AT. The sharp peak observed at 128.39 ˚C of DTA trace evidences the melting point of the sample. Interestingly, the melting point of ATMB is much greater than ATZC (58 ˚C) [7] and ATCC (110 ˚C) [16].

3.7 Scanning Electron Microscope (SEM)

Figure 5 shows the surface morphology of as grown single crystals of ATMB. The photograph was recorded in the operating voltage of 20 KV with the magnification factor of 1000. From the photograph, it is observed that the basic units are arranged in different layers, which is a clear evidence for the stacking of fundamental units during crystal growth
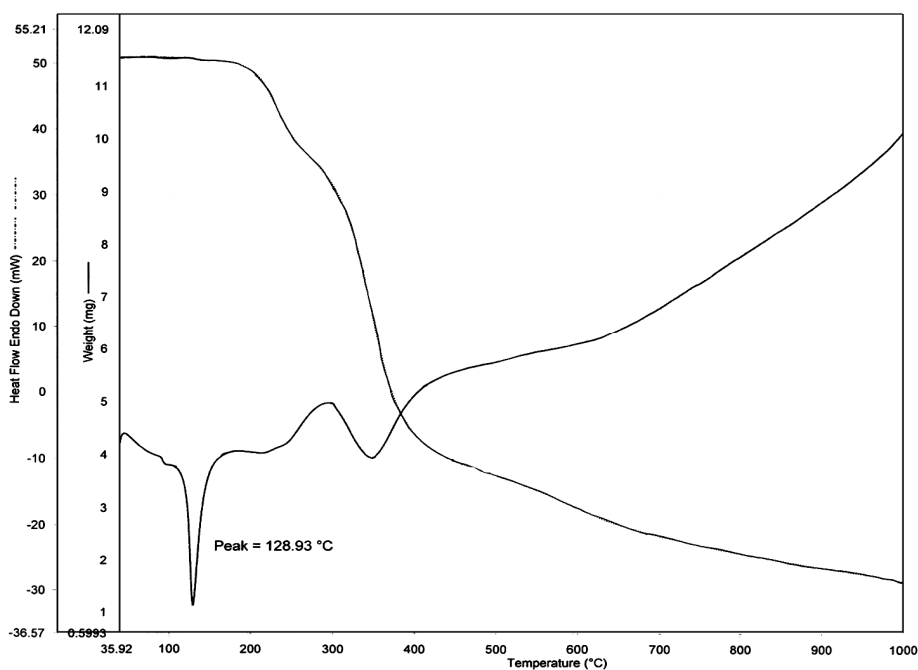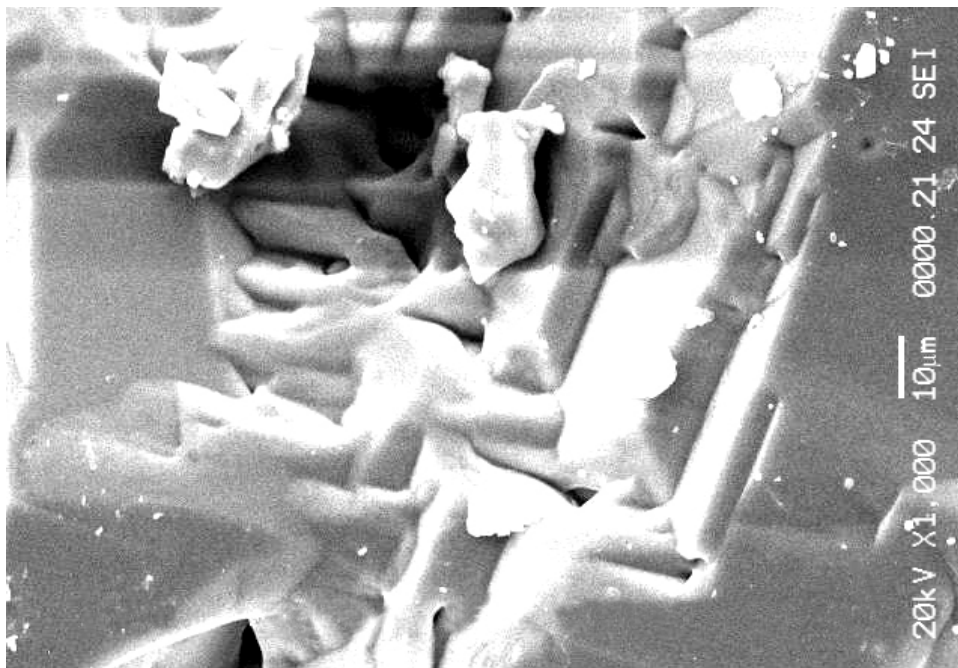

Fig.4. TGA-DTA trace of ATMB single crystal

_____

Fig. 5. SEM photograph of ATMB single crystal

3.8 Photoluminescence

The photoluminescence (PL) spectrum of ATMB single crystal is shown in Fig. 6. The excitation of the sample is observed between the region 200 to 300 nm and the emission between the region 300 to 800 nm. The absorption of the sample starts around 247 nm and it decreases upto 280 nm and then maintained a constant with very less absorption (less than 0.5 unit). When excited with 235 nm radiation, the sample emits a sharp band at 433 nm, which corresponds to the metal (Hg) – blue spectral lines. After this emission, a small absorption peak is observed at 504 nm, which may be due to the transition between metal (Hg) and the sulphur present in the ligand (AT). The green emission is also observed around 528 nm.

3.9 Dielectric Mesurement

Suitably cut and polished section of ATMB was subjected to dielectric studies. The measurements were made on the (001) face of the sample by varying the frequency from 50 Hz to 5 MHz at different temperatures (308 K, 328 K, 348 K, 368 K and 388 K). Figs. 7 and 8 show the variations of dielectric constant and dielectric loss with log frequency. It is found that the dielectric constant of ATMB is high at low frequencies and it decreases with increasing frequency and dielectric constant increase with temperature and a similar trend is observed in the dielectric loss (Fig. 8). In ATMB, at 50 Hz, the value of dielectric constant is found to be around 55 (308 K) and above 10 kHz, the value of dielectric constant remaining unchanged upto 5 MHz. At low frequencies, all the four contributions are active hence higher dielectric constant. The decrease in dielectric constant with increase in frequency may be attributed to the dependence on the electronic, ionic, orientational and space charge polarizations. In the lower frequency region,

177

_____

dielectric loss is more due to the loss associated with ionic mobility [17]. The low dielectric loss with high frequency implies that the sample possesses good optical quality with lesser defects.
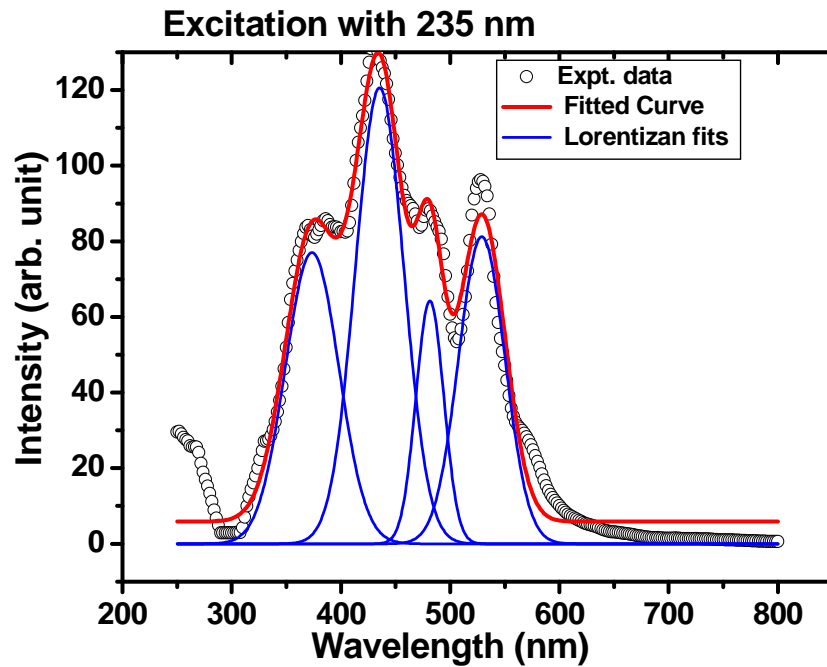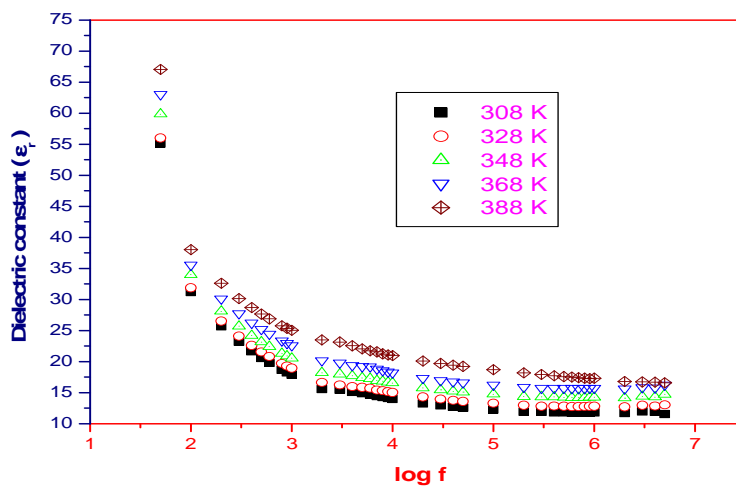

Fig. 6. PL spectrum of ATMB single crystal

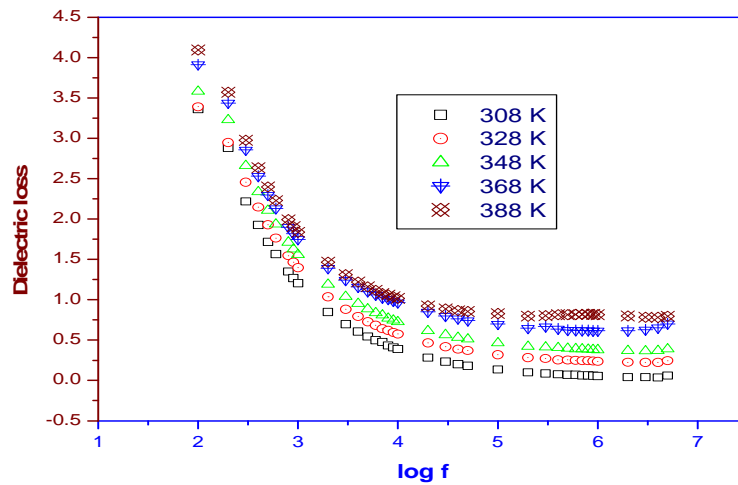**Fig. 7. Variation of dielectric constant with log frequency at different temperatures for ATMB crystal**

_____

**Fig. 8. Variation of dielectric loss with log frequency at different
temperatures for ATMB crystal**

3.10 DC Conductivity

The *dc* electrical conductivity measurements were carried out for the ATMB crystal using the conventional two-probe technique in the temperature range 313 - 423 K. The *dc* electrical conductivity (σ_{dc}) of the crystal was calculated using the relation

$$\sigma_{dc} = t/RA$$

where R is the measured resistance in ohm, t is the thickness of the sample and A is the area of face in contact with the electrode. The σ_{dc} values were fitted into the equation

$$\sigma_{dc} = \sigma_o \exp(-E_d/kT)$$

Electrical conductivity depends on thermal treatment of a crystal. The σ_{dc} values in the temperature region studied are found to increase with temperature for the sample. The electrical conduction is mainly a defect controlled process in low temperature region. It is observed from the Fig. 9, the electrical conduction of ATMB is low at lower temperature owing to trapping of some carriers at defect sites which is predominantly due to moment of defects produced by thermal activation.   The value of conductivity *ln* σ_{dc} is found to increase with temperature. Activation energy was found to be 0.3 eV from the plot (Fig. 9).

3.11 Microhardness Studies

Microharness studies were carried out by selecting smooth face and free from any microstructures or defects of the ATMB single crystals were selected. The Vickers Hardness Numbers (H_v) were observed for the applied load of 5, 10, 15, 25 and 30g. The indentation time was kept as 15 sec for each load. Micro cracks were observed in the sample due to the mechanical stress when a load of 35 g was added. Fig. 10 shows the plot of applied load (p) Vs Vickers Hardness Number (H_v). From the plot, it is observed that the hardness number increase

179

_____

with increase in applied load. The work hardening coefficient of ATMB was calculated by drawing a plot between log p and log d, and it is found to be 3.57.

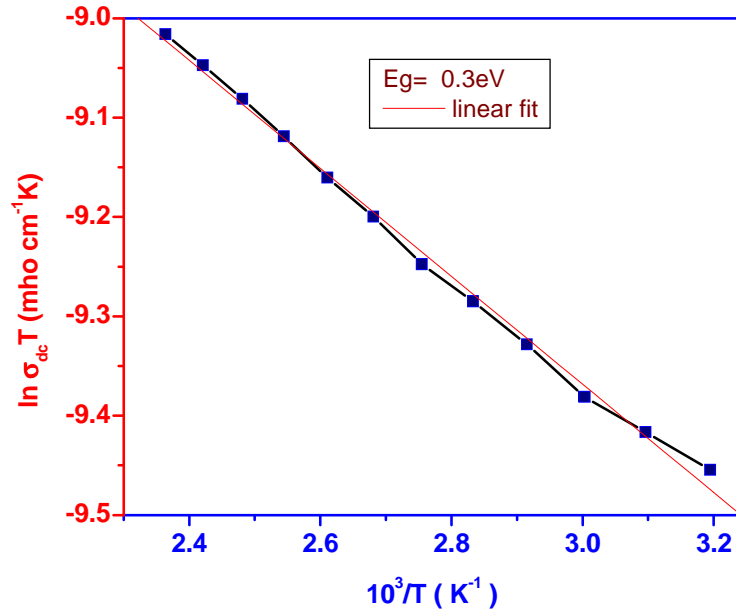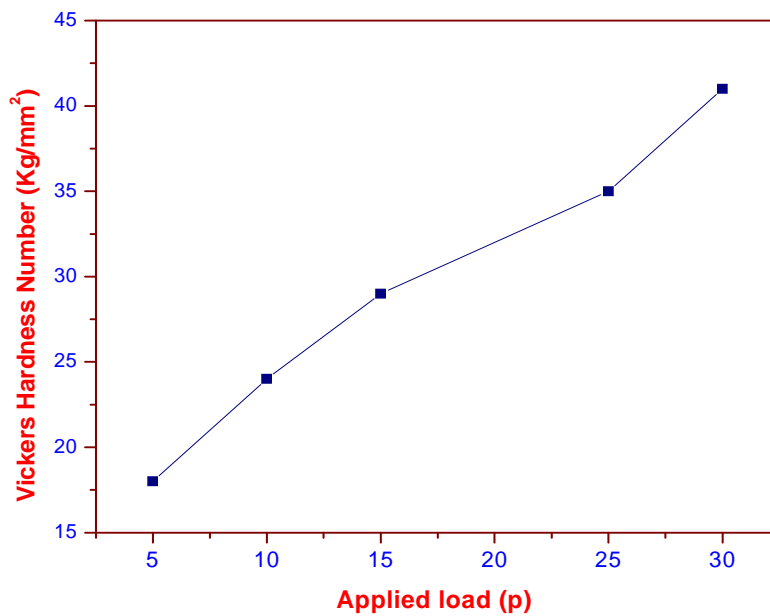**Fig. 9. Plot of ln(σ_{dc})T versus 1000/T for ATMB single crystal**

Fig. 10. Variation of Vickers hardness number with the applied load

_____

CONCLUSION

Single crystals of ATMB with appreciable size were conveniently grown by the slow evaporation technique in room temperature for the first time. The structure of the grown crystal was confirmed by single crystal XRD. ATMB belongs to trigonal crystal system with the space group, R3c. The incorporation of carbon, hydrogen and nitrogen was estimated and compared with the theoretical values. The UV cut-off wavelength of ATMB lies around 350 nm and the band gap energy of the sample is found to be 3.9280 eV. Thermal studies reveal that the melting point of the sample is 125.11 ˚C, which is higher than other complexes of allylthiourea. Activation energy of the sample was calculated by *dc* conductivity measurements and is found to be 0.3 eV. The grown crystals were also subjected to dielectric, microhardness, SEM and photoluminescence studies.

REFERNCES

[1] D. Xu, M.H. jiang, Z.S. Shao, *Synth. Crystal*, 16 (**1987**) 1.

[2] S. Selvakumar, S.M. Ravi Kumar, K. Rajarajan, A. Joseph Arul Pragasam, S. A. Rajasekar, K. Thamizharasan and P. Sagayaraj, *Crystal Growth & Design*, 6 (**2006**) 2607.

[3] Ginson. P. Joseph, J. Philip, K. Rajarajan, S.A.Rajasekar, A. Joseph Arul Pragasam, K. Thamizarasan, S. M. Ravi Kumar, P.Sagayaraj, *Journal of Crystal Growth*, 296 (**2006**) 51.

[4] K. Rajarajan, Preema C. Thomas, I. Vetha Potheher, Ginson P. Joseph, S.M. Ravi Kumar, S. Selvakumar and P. Sagayaraj, *Journal of Crystal Growth*, 304 (**2007**) 435.

[5] Hou Wenbo, Yuan Duorong, Xu Dong, Zhang Nan, Yu Wentao, Liu Mingguo, Tao Xutang, Sun Suoying and Jiang Minhua *J. Crystal Growth*, 133 (**1993**) 71.

[6] Ginson P. Joseph, K. Rajarajan, J.Madhavan and P. Sagayaraj, *Materials Research Bulletin*, 42 (**2007**) 2040.

[7] H. Q. Sun, D. R. Yuan, X. Q. Wang, X. F. Cheng, C. R. Gong, M. Zhou, H. Y. Xu, X. C. Wei, C. N. Luan, D. Y. Pan, Z. F. Li and X. Z. Shi, *Cryst. Research Technol.*, 40 (**2005**) 882.

[8] W. B. Hou, M. H. Jiang, D. R. Yuan, D. Xu, N. Zhang, M. G. Liu and X. T. Tao *Mat. Res. Bull.,* 28 (**1993**) 645.

[9] D.R. Yuan, N. Zhang, W.T. Yu, D. Xu, X. T. Tao and M. H. Jiang, *Chinese. J. Lasers,* 17 (**1990**) 332.

[10] S. K. Kurtz and T. Perry, *J. Appl. Phys,* 39 (**1968**) 3798.

[11] Tauc J., (**1974**), 'Amorphous and Liquid semiconductors', *J. Tauc Ed. Plenum*, New York.

[12] N. Zhang, D. R. Yuan, X. T. Tao, D. Xu, Z. S. Shao and M. H. Jiang, *Chinese Sci. Bull.,* 15 (**1989**) 1154.

[13] B. Narayana Moolya, A.Jeyarama, M.R. Suresh Kumar, S. M. Dharmaprakash, *J. Crystal Growth*, 280 (**2005**) 581.

[14] A. Pricila Jeyakumari, J. Ramjothi, S. Dhaniskodi, *J. Crystal Growth*, 269 (**2004**) 558.

_____

[15] Toshiyuki Masui, Takanobu Chiga, Nobuhito Imanaka and Gin-Ya Adachi *Mat. Res. Bull.*, 38 (**2003**) 17.

[16] H. Q. Sun, D. R. Yuan, X. Q. Wang, Y.Q. Lu, Z.H. Sun, X.C. Wei, X.L. Duan, C. N. Luan, M.K. Lu, D. Xu, *J. Crystal Growth*, 256 (**2003**) 183.

[17] H. Shinichi, C. K. Pan, O. Hiroshi and I. Yoshihiro, *J. Mater. Sci.*, 25 (**1990**) 2800.